TẠP CHÍ KHOA HỌC
TRƯỜNG ĐẠI HỌC QUY NHƠN

Ảnh hưởng của liều lượng phân hữu cơ vi sinh đến sinh trưởng, năng suất và chất lượng quả của giống bí đao Mỹ Thọ trồng trên đất sỏi tại Hoài Hương, Hoài Nhơn, Bình Định

Nguyễn Triết[1,*] , Võ Minh Thứ[2]

[1]THPT Nguyễn Du, Hoài Nhơn, Bình Định, Việt Nam
[2]Khoa khoa học tự nhiên, Trường Đại học Quy Nhơn, Việt Nam

Ngày nhận bài: 21/09/2021; Ngày nhận đăng: 12/11/2021

TÓM TẮT

Nghiên cứu nhằm đánh giá ảnh hưởng của liều lượng phân hữu cơ vi sinh (HCVS) đến sinh trưởng, năng suất và chất lượng quả của giống bí đao Mỹ Thọ trồng trên đất sỏi ở phường Hoài Hương, thị xã Hoài Nhơn, tỉnh Bình Định. Thí nghiệm được thiết kế với ba mức bón phân HCVS (400, 500, 600 kg/ha). Đất trồng thí nghiệm có độ pH chua (4,4), chất hữu cơ tổng số, hàm lượng nitơ và kali dễ tiêu ở mức nghèo. Kết quả thí nghiệm cho thấy, bón bổ sung phân HCVS cho giống bí đao Mỹ Thọ với mức 600 kg/ha có tác động tốt đến một số chỉ tiêu hóa sinh, năng suất và chất lượng quả. Hàm lượng chất khô trong quả bí tăng từ 0,15% - 1,48%, hàm lượng vitamin C tăng từ 0,2% - 5,29%, axít hữu cơ tổng số tăng từ 13,97% - 40,53% và độ Brix tăng từ 0,09% - 1,2%. Bón bổ sung phân HCVS đã làm năng suất cao hơn khi so với đối chứng từ 4,72 - 19,9 tấn/ha, lợi nhuận tăng từ 30,8 - 130,3 triệu/ha. Hiệu quả cao nhất ở mức bón 600 kg/ha. Kết quả đạt được của nghiên cứu giúp khuyến nghị người trồng bí đao Mỹ Thọ nói riêng và bí đao nói chung bón bổ sung phân HCVS tạo ra sản phẩm có chất lượng đảm bảo, an toàn cho người sử dụng và cung cấp nguyên liệu cho sản xuất bánh kẹo và nước giải khát.

Từ khóa: *Bí đao Mỹ Thọ, chỉ tiêu hóa sinh, năng suất, chất lượng, phân HCVS.*

**Tác giả liên hệ chính.*
Email: trietnd@gmail.com

JOURNAL OF SCIENCE
QUY NHON UNIVERSITY

Effect of micro-organic fertilizers on some growth norms, yield and fruit quality of My Tho gourd variety grown in gravel soil of Hoai Huong, Hoai Nhon, Binh Dinh province

Nguyen Triet[1,*] , Vo Minh Thu[2]

[1]Nguyen Du high school, Hoai Nhon, Binh Dinh, Viet Nam
[2]Faculty of Natural Sciences, Quy Nhon University, Viet Nam

Received: 21/09/2021; Accepted: 12/11/2021

ABSTRACT

The study was carried out to evaluate the effect of micro-organic fertilizer (MOF) on growth, yield and quality of My Tho gourd variety grown in gravel soil of Hoai Huong commune, Hoai Nhon district, Binh Dinh province. This study used MOF at dosages of 400, 500 and 600 kg.ha^{-1}. Experimental soil was analyzed in terms of pH (4,4), total organic matter, content of available nitrogen, and potassium at low level. The biochemical norms such as chlorophyll content, total nitrogen, protein, total sugar, and vitamin C were determined. The research results showed that the application of MOF at dosages of 400, 500, 600 kg.ha^{-1} increased some biochemical norms, productivity and fruit quality. Dry matter content in fruit increased from 0.15% to 1.48%, vitamin C increased from 0.20% to 5.29%, protein increased from 0.74% to 1.38%, total organic acids increased from 13.97% to 40.53% and Brix increased from 0.09% to 1.20%. The adding of MOF increased fruit productivity from 4.72 - 19.09 tons. ha^{-1} and the profit increased from 30.840 to 130.33 million VND, which was higher than that of the control without applying MOF. The best effect is at dosage of 600 kg.ha^{-1}. The research results recommend that gourd growers should use MOF to produce quality and safe products for consumers, and provide a raw material source for the food and beverage industry.

Keywords: *My Tho gourd variety, biochemical norms, yield, quality, micro-organic fertilizer.*

1. INTRODUCTION

Among vegetables, gourd (*Benincasa hispida*) which belongs to the family *Cucurbitaceae*, also known as long green squash, lemon squash, etc., is a relatively common crop. For a long time, gourd fruit has been used as food for family meals such as soup and stir-fry. In addition, gourd is also a source of raw materials for the production of cakes, jams, candies and soft drinks, with a high export value.[1,13] Gourd has the ability to grow, develop well, adapt widely, tolerate pests and diseases very well. Pumpkin cultivation supplies little or no pesticides, so gourd is considered a clean and safe product for human health. The pericarp of gourd is thick and hard, so it is easy to be preserved for a long time, and to be transported easily. In addition, pumpkin also is material to supply for companies and factories to process and create products from gourd. Pumpkin is also a vegetable to

**Corresponding author.*
Email: trietnd@gmail.com

https://doi.org/10.52111/qnjs.2022.16108

be kept in reserve for the next season, which is very convenient for the people living in regions lacking vegetables.

Pumpkin has a very rich nutrient content, and it is used to make very delicious foods, so gourd is widely grown in Vienam. The product and yield of gourd depends on varieties, agrochemical conditions, soil, weather and cultivated techniques. However, fertilizers play an important role in long term planting, increasing yield, increasing resistance to pests and diseases for gourd plants and increasing nutrients for the soil. Nevertheless, using unbalanced and unsuitable chemical fertilizer will depress the growth and development of crops in general and of gourds in particular, and it also degrades the planted soil.

Many different gourd varieties have been grown in Binh Dinh, but the My Tho gourd variety is considered a local gourd variety with an average fruit weight of 40-60 kg per fruit. The skin of the young fruit has a green banana color, but when it is old, the rind turns dark green. The flesh of the fruit is thick, fragrant and delicious, but it has not been widely planted by the farmers.

In order to increase the yield of gourd, in addition to choosing good varieties, high yield, and cultivated area, the supply of reasonable fertilizer also plays an important role in improving yield and output. Currently, farmers in My Tho mainly use chemical fertilizers, and rarely use micro-organic fertilizer (MOF). The Institute of Agricultural Science and Technology of the South Central Coast implemented the project "Exploiting and developing the genetic resources of pumpkin in the South Central Coast" (2011 - 2012) in order to restore, develop and build cultivation techniques of large-fruited gourd variety in the South Central Coast region.[7] However, the project only studies NPK fertilizer levels combined with manure.

As mentioned above, the use of microbial organic fertilizers is essential. MOF not only fully adds nutrients to plants, but also helps the soil retain moisture, stay fresh, retain water and help plant roots be healthy. In addition, MOF also helps the micro-organism in the soil to thrive, helping plants to better absorb nutrients.

Currently, there is no research on MOF for My Tho gourd in Binh Dinh province. Therefore, studying the effect of MOF on growth, fruit yield and quality of My Tho gourd variety grown on gravel soils in Hoai Huong, Hoai Nhon is necessary and it will contribute to prove the technical process for growers to produce clean products for users in the local and near regions.

2. MATERIALS AND METHODS

2.1. Experimental materials

The research was conducted on My Tho gourd variety, which has a growth period of 5 to 6 months and an the average fruit weight of 45 to 60 kg. The seeds were taken from Chanh Trach village, My Tho commune, Phu My district, Binh Dinh province.

The microbial organic fertilizer used is Song Gianh fertilizer. Ingredients include: organic matter (15%), humic acid (2.5%); effective P_2O_5 (1.5%); Ca, Mg, S (0.3% - 1.0%); microbial composition: *Bacillus* 1×10^6 CFU/g; *Azotobacter:* 1×10^6 CFU/g; *Aspergillus* sp: 1×10^6 CFU/g.

2.2. Experimental methods

The experiment was carried out in the winter - spring 2020 - 2021 crop in Hoai Huong commune, in Hoai Nhon town of Binh Dinh province, including four treatments (Treat.) with different dosages of MOF. Basal fertilizes (BF_S) consist of 2 tons of manure + 500 kg of lime + 100 kg of NPK 16:8:16 per hectare.

Treatment 1: BFs + 400 kg MOF.ha^{-1}

Treatment 2: BFs + 500 kg MOF.ha^{-1}

Treatment 3: BFs + 600 kg MOF.ha^{-1}

Treatment 4 (control): BFs + 0 kg MOF.ha^{-1}

The area of each experimental plot was 15 m^2, replicated three times, and the total area was 180 m^2. The experiment was laid out as a randomized complete block design (RCBD). The size of a hole was 60 cm in width and

40 cm in height. The distance between plants was 25 cm, planting 15 plants per plot.

Holes were dug and plants were fertilized with 100% basal fertilizers + 50% MOF + 20% NPK according to each treatment, mixing well with soil, covering with soil in 7 days before planting.

The first additional fertilizer was applied when the plant height reached 20 - 35 cm with 30% MOF + 30% NPK fertilizer, combined with soil cultivation. The second additional fertilizer was applied when the length of stem reached 100 - 150 cm with 20% MOF + 30% NPK. The third additional fertilizer was applied when the plant was flowering and forming fruit with 20% NPK.

Indicators and measures

Humus content was analyzed according to Walkley - Black method, exchanged acidity according to Daikuhara - Cononova method, available nitrogen according to Chiurin and potassium contents according to and Kiecxanov method.[6]

The total growing time (days) was determined from sowing to 80% of plants harvested .

The height of the main stem (cm) was determined by using a ruler to measure from base to apex when the plant had 5 actual leaves and was flowering.

The dry matter content (%) was measured by drying at 105 ^{o}C and reweighing until constant mass. Total organic acid content (mg.100g^{-1} fresh matter) was analyzed according to Ecmacov method.[6]

The brix degree (%) or total dissolved organic matter content was determined using a handle Brix refractometer.

The Vitamin C content (mg.100g^{-1} fresh weight) was determined by using Iodine solution to titrate.[3]

The total starch content (% fresh matter) was determined by starch hydrolysis and quantification of reducing sugars according to Bertrand[3] method.

The chlorophyll content (mg.g^{-1} fresh leaves) was analyzed by spectrophotometric method.[3]

The content of water and dry matter in leaves was determined by drying at 105 °C before flowering and after fruit set.[3] The total nitrogen content (%) was determined by the method of Micro Kjeldahl.[6]

Theoretical yield (tons per ha) = Number of plants.m$^{2.-1}$ x fruit weight (kg) x number of fruits per each plant x 10. Actual yield (tons per ha) = Weigh the total fruit mass per experimental treatment (kg), then converting it to tons per ha.

The obtained data were statistically processed by MS software, Excel 2010 and Statistix version 8.0. Differences between mean values were calculated using the LSD test method at the significance level of 0.05.

3. RESULTS AND DISCUSSION

3.1. Agrochemical norms of experimental soil before and after planting

Table 1. Some agrochemical norms of experimental soil before and after planting

Norms	Soil before planting	Soil after planting			
		Treat.1	Treat.2	Treat.3	Treat.4 (control)
Humus content (% dry weight)	0.78	1.46	1.93	2.65	1.69
pH (KCl)	4.40	5.20	5.40	5.75	5.10
available nitrogen content (mg.100g^{-1} dr.w.)	1.02	1.14	1.61	1.14	0.88
Available potassium content (mg.100g^{-1} dr.w.)	7.11	25.43	12.29	12.05	14.82
Exchange acidity (meq.100g^{-1})	0.18	0.12	0.1	0.1	0.1

https://doi.org/10.52111/qnjs.2022.16108

The content of substances in the soil before and after the experiment did not change. Specifically, before planting, the soil had not been fertilized with microbial organic fertilizer, the humus content in the soil accounted for 0.78% of dry matter, belonging to the group of very poor humus soils. The content of easily digestible nitrogen and potassium in the soil was 1.02 mg.100g^{-1} dry weight and 7.11 mg.100g^{-1} of K_2O, respectively, the pH value was 4.40. After planting, all three experimental treatments increased compared to the control, reaching from 1.46 to 2.56%, available nitrogen content increased from 0.12 to 0.59 mg.100g^{-1}, easily digestible potassium content increased from 4.94 to 18.32 mg.100g^{-1} dry matter compared to the soil before planting.

The application of MOF has increased the humus content of the planting soil at rich levels because the MOFs contain humic acids and organic matter. In addition, MOF also contains microbial strains of *Bacillus, Azotobacter, Aspergillus* and nutrients such as humus, Ca, P, Mg, S that helped to convert organic matter in the soil into humus, available nitrogen and potassium making plants absorb better. Moreover, it also improved pH, reduced acidity (pH increased from 5.20 - 5.75).

3.2. Some biochemical parameters in gourd leaves before flowering and fruit set

3.2.1. Chlorophyll content in gourd leaves

Results of analysis of chlorophyll content in gourd leaves at the seedling stage before flowering and fruit formation are presented in Table 2.

Table 2. Chlorophyll content in gourd leaves

	Chlorophyll (a+b) before flowering		Chlorophyll (a+b) at fruiting stage	
	(mg.g^{-1} fresh leaves)	% compare with control	(mg.g^{-1} fresh leaves)	% compare withcontrol
Treat.1	2.42^{a}	102.98	3.16^{b}	128.98
Treat.2	2.52^{a}	107.23	3.44^{b}	140.41
Treat.3	2.77^{a}	117.87	4.08^{a}	166.53
Treat.4 (Control)	2.35^{a}	100.00	2.45^{c}	100.00
CV (%)	**14.12**		**8.25**	
LSD$_{0.05}$	**0.71**		**0.54**	

Note: *Mean followed by the same letter isn't significantly different within the columns according to LSD test at a 5% significance level; CV: coefficient variance.*

At the seedling stage, the leaf total chlorophyll content in the experimental treatments ranged from 2.35 to 2.77 mg.g^{-1} fresh weight; the highest is in Treat.3 (2.77 mg.g^{-1}), which increased 17.87% compared with that of the control (2.35 mg.g^{-1}). However, there was not statistically significant difference for the total chlorophyll content between the experimental treatments at the 5% level.

At the stage of fruit formation, the chlorophyll (a + b) content in the gourd leaves in the treatments with MOF was higher than that in the control plants, increasing from 28.98 to 66.53%. In which, at a dosage of 600 kg per ha, the highest value was achieved (4.08 mg.g^{-1} fresh leaves) and the lowest was in the control without treatment of MOF (2.45 mg/g fresh leaves). The difference for chlorophyll content in all treatments with MOFcompared to the control (without MOF) was statistically significant.

3.2.2. Dry matter and water content in gourd leaves

The dry matter content of My Tho gourd leaves in the experimental plants through the two stages before flowering and fruit set is shown in Table 3.

Table 3. Dry matter content in gourd leaves over two stages

	Leaf total water content (%)		Dry matter content (%)	
	Stage before flowering	Fruiting stage	Stage before flowering	Fruiting stage
Treat.1	85.14^{b}	82.22^{ab}	14.86^{b}	17.78^{ab}
Treat.2	84.88^{bc}	81.60^{b}	15.12^{ab}	18.40^{a}
Treat.3	83.45^{c}	80.72^{b}	16.51^{a}	19.28^{a}
Treat.4 (control)	87.53^{a}	84.02^{a}	12.47^{c}	15.98^{b}
CV (%)	**0.91**	**1.18**	**5.29**	**5.43**
$LSD_{0.05}$	**1.56**	**1.93**	**1.6**	**1.9**

Note: *Mean followed by the same letter isn't significantly different within the columns according to LSD test at a 5% significance level; CV: coefficient variance.*

***Pre-flowering period**:* The dry matter content in the leaves of the gourd in the experimental plants ranged from 12.47 to 16.51%, the highest in Treat.3 (16.51%), followed by Treat.2 (15.12%), Treat.1 (14.86%) and the lowest in the control (12.47%). There was a statistically significant difference in the dry matter content in the treatments with MOF compared with the treatment without supply microbial organic fertilizer. Total water content in leaves reached from 83.45 to 87.53%, the control treatment is highest (87.53%) and lowest in Treat.3 (83.45%).

***Fruit formation period**:* The dry matter content in the gourd leaves in the experimental plants fertilized with MOF was higher than that in the control plants. The dry matter content in the leaves ranged from 17.78% to 19.28%. The highest is in Treat.3 (19.28%) and lowest in the control (15.98%).

Similarly, the total water content in leaves also ranged from 80.72% to 84.02%. The lowest is in Treat.3 (80.72%) and the highest in Treat.4 (84.02%). The difference in total water content between Treat.2, Treat.3 and Treat.4 is statistically significant at 5%; between Treat.3 and Treat.1, Treat.2 is not significantly different.

Thus, MOF has increased the total chlorophyll content (Table 2), thereby, increasing the intensity of photosynthesis which leads to an increase in dry matter content in leaves. The results of this study are consistent with the reports of many other authors.[7 - 10]

3.2.3. Total nitrogen content in gourd leaves through two growth and development periods

The effect of HCVS MOF on the total nitrogen content of leaves during the pre-flowering and fruiting stages is indicated in Table 4.

Table 4. Leaf total nitrogen content

	Total nitrogen content in leaves (%)	
	Pre-flowering period	The period of fruit plants
Treat.1	4.66	3.75
Treat.2	4.55	3.75
Treat.3	4.34	3.75
Treat.4 (control)	4.45	4.24

https://doi.org/10.52111/qnjs.2022.16108

The data from Table 4 showed that: In the pre-flowering period, the total nitrogen content of leaves in all experimental treatments ranged from 4.34 to 4.66%, and the difference between the experimental treatments is not considerable, only from 0.10 to 0.32%. At the period of fruit formation, the total nitrogen content in leaves is lower than that before flowering, ranging from 3.75 to 4.24%. This is explained that it is possible that at the fruiting stage, nitrogen containing organic substances such as amino acids, proteins, etc., are transported to the fruit for storage, therefore reducing the amount of nitrogen in the leaves.[13,14]

3.3. Growth and development indicators of gourd

The effect of microbial organic fertilizer application on the duration of growth, development, and height of gourd plants in different stages is shown in Table 5.

Table 5. Duration of growth and development of gourd plants

	Time from sowing to stages (days)			
	Sowing seeds to 5 leaves	**Sow seeds to flowering**	**Sowing seeds to fruit formation**	**Total growing duration**
Treat.1	18	53	67	157
Treat.2	16	57	72	162
Treat.3	16	59	77	175
Treat.4 (control)	19	51	64	148

The data in Table 5 indicated that:

The period from sowing to 5 young leaves: The root system of the plant had not yet developed strongly and nutrients from the environment had a great influence on the plant, so the growth rate was almost the same.

At the flowering stage, the addition of MOF had a great impact on the growth time and development of gourd plants. The number of days from seed sowing to flowering in each experimental treatment was different. Specifically, the number of days from planting to flowering in the experimental plants fluctuated from 51 to 59 days. In which, the Treat.4 (control) had the fastest flowering time (51 days), and Treat.3 (supplied 600 kg.ha^{-1}), the slowest flowering time (59 days).

The time from planting to fruiting in Treat.4 was the fastest (64 days), the slowest was in Treat.3, applying 600 kg.ha^{-1} (77 days). The growth in Treat.1 (400 kg.ha^{-1}) and Treat.2 (500 kg.ha^{-1}) reached 67 and 72 days, respectively. Thus, the application of MOFs at different dosages also had different effects on the growth time, flowering and fruit formation of My Tho gourd plants.

The growth duration of gourd in the experimental treatments ranged from 148 to 175 days, in which the period from planting to harvesting the fruit was the shortest (148 days) in Treat.4, next 157 days in Treat.1 (400 kg.ha^{-1}), 162 days in Treat.2 (500 kg.ha^{-1}) and longest growing time (175 days) in Treat.3 (600 kg.ha^{-1}). Thus MOF has provided plants with a lot of organic matter, humus, macronutrient and micronutrient elements which take more time for plants to absorb, so the growth duration is longer.

The dose of microbial organic fertilizer affects the main stem length of gourd plants, shown in Table 6.

Table 6. Pumpkin stem length at seedling stage and fruit formation

	Seedling stage		Fruit forming stage	
	Stem length (cm)	% compare with control	Stem length (cm)	% compare with control
Treat.1	11.09[b]	111.79	172.07[b]	108.80
Treat.2	12.25[b]	124.49	174.53[b]	109.63
Treat.3	14.26[a]	144.92	186.40[a]	117.09
Treat.4 (DC)	9.84[c]	100.00	159.20[c]	100.00
CV (%)	**8.01**		**5.76**	
$LSD_{0.05}$	**0.70**		**7.31**	

Note: *Mean followed by the same letter isn't significantly different within the columns according to LSD test at a 5% significance level; CV: coefficient variance.*

Table 6 showed that at the seedling stage, there are 5 leaves; the stem length in the treatments fluctuated from 9.84 to 14.26 cm. The plant height in treatments with MOF is higher than in the control treatment, the highest in Treat.3 (600 $kg.ha^{-1}$) is 14.26 cm, increasing 44,92% compared to the control. In the period of fruit formation, the length of the gourd stem in the treatments ranged from 159.20 to 186.40 cm. In which, the length in Treat.3 reached the largest (186.40 cm), the difference was statistically significant at 5% compared with the control (159.20 cm). Thus, through the two periods, it was shown that the length of gourd plants in the treatments with MOF was higher than in the control treatment and the difference was statistically significant.

The application of micro organic fertilizers had added nutrients and micro-organisms, helping the process of converting unavailable compounds into available, making the gourd better absorb nutrients. Therefore, plant growth had been improved. When applying MOF at a large dosage, the growth time was prolonged, so the plant height was higher.[2,13,14]

3.4. Some quality indicators of fruit

3.4.1. Total water and dry matter content in fruit

Table 7. Total water and dry matter content

	Total water (%)	Dry matter (%)
Treat.1	95.31[a]	4.69[a]
Treat.2	96.28[a]	3.72[a]
Treat.3	94.95[a]	5.05[a]
Treat.4 (control)	96.43[a]	3.57[a]
CV(%)	**1.13**	**25.42**
$LSD_{0.05}$	**2.16**	**2.16**

Note: *Mean followed by the same letter isn't significantly different within the columns according to LSD test at a 5% significance level; CV: coefficient variance.*

As can be seen in Table 7, the total water content in fruit accounted for up to 94% of fruit weight, fluctuating from 94.95% to 96.43%, in which, the lowest (94.95%) is in Treat.3 and the highest in Treat.4. (96.43%). Similarly, the dry matter content of gourd fruit in the experiment only fluctuated from 3.57 to 5.05). Treatments with MOF, the dry matter content of fruit was higher than that in the control. The dry matter content in Treat.3 was the highest (5.05%), followed by Treat.1 (4.69%) and lowest in Treat.4 (3.57%). Thus, the application of MOF for gourd had a good effect on the accumulation of dry matter in the fruit, of which Treat.3 was the best.[10]

https://doi.org/10.52111/qnjs.2022.16108

3.4.2. Total sugar, total organic acid and vitamin C, total soluble organic matter, Brix degree in fruit

For plants, sugar provides energy and is an important building block in cells, tissues and organs. Vitamin C participates in the implementation of redox reactions, necessary for the synthesis of collagen (the intercellular connective substance in the vessel walls, connective tissue, bones, teeth...). Animals cannot synthesize vitamin C; the source of vitamin C in animals is provided from plants.[1,4,5] Organic acids play an important role in amino acid synthesis and other biochemical reactions. Therefore, the content of sugar, organic acids and vitamin C are important indicators to evaluate the quality of vegetables and fruits.[11]

The analyzed data of total sugar, organic acid, soluble organic matter, vitamin C and Brix degree in fruit are shown in Table 8.

Table 8. Total sugar content, vitamin C, total soluble organic matter

CTTN	Total sugar (% fresh matter)	Total organic acids (mg.100g^{-1} fresh weight)	Vitamin C (mg.100g^{-1} fresh weight)	Brix degree (%)
Treat.1	0.11	233.24^{bc}	46.26^{bc}	2.0
Treat.2	0.12	239.88^{b}	49.53^{ab}	2.1
Treat.3	0.28	259.80^{a}	51.35^{a}	2.3
Treat.4 (control)	0.09	219.27^{c}	46.06^{c}	1.1
CV (%)		**3.96**	**3.5**	
LSD$_{0.05}$		**18.84**	**3.38**	

Note: *Mean followed by the same letter isn't significantly different within the columns according to LSD test at a 5% significance level; CV: coefficient variance.*

The total sugar content in the fruit in different samples was not significantly different, ranging from 0.09 to 0.28% of fresh matter. The content of total organic acid in the experimental treatments was significantly different; the highest was in Treat.3 (259.8 mg.100g^{-1}), and the lowest in the control (219.27 mg.100g^{-1}). The difference between organic acid content in fruit in Treat.3 and Treat.2 and that of the control was statistically significant. Organic acid content of fruit in the experiments with MOF were higher than in the control. The content of vitamin C in the fruit in the treatments with micro organic fertilizers were not much different from that in the control treatment, only from 0.20 to 5.29 mg.100g^{-1}of fresh weight, the most in Treat.3 (600 kg.ha^{-1}). The total soluble organic matter content in the fruit ranged from 1.1 to 2.3% of fresh matter, of which the highest in Treat.3 (2.3%) and the lowest in the control (1.1%). Thus, in the experimental plants fertilized with MOF, the total soluble organic matter content accumulated in the fruit was higher than that in the control treatment.

The above results showed that the concentration of nutrients (organic acids, total sugar, vitamin C, total soluble organic matter) accumulated in My Tho gourd fruit in experimental plants with MOF was higher than that in fruit of the control. Thus, the addition of MOF made the gourd plant absorb nutrients better, increasing the metabolic rate,[8,10,11] which led to an increase in the accumulation of organic substances in the fruit. Moreover, among the experiments with different dosages of fertilizers, the nutrients content was higher with the application rate of 600 kg.ha^{-1} compared with that of 400 and 500 kg.ha^{-1}. Thus, the supply of 600 kg.ha^{-1} is suitable for the growth, synthesis and accumulation of nutrients of My Tho gourd.

3.5. Components of yield of gourd

3.5.1. Number of fruits per plant and average weight of each fruit

Table 9. Number of fruit and average weight of each fruit

	Number of fruits per plant		Average weight of each fruit	
	Number of fruits	% compare withcontrol	Weight (kg)	% compare withcontrol
Treat.1	2.73[b]	157.80	22.10[b]	146.16
Treat.2	3.27[b]	189.02	22.21[b]	146.89
Treat.3	4.73[b]	273.41	28.01[a]	185.25
Treat.4 (control)	1.73[c]	100.00	15.12[c]	100.00
CV (%)	**20.82**		**18.46**	
$LSD_{0.05}$	**0.75**		**3.59**	

Note: *Mean followed by the same letter isn't significantly different within the columns according to LSD test at a 5% significance level; CV: coefficient variance.*

The number of fruits per plant in the experiments obtained from 1.73 to 4.73 fruits, the highest (4.73 fruits) in Treat.3 and the lowest in Treat.4 (1.73). The difference in the number of fruits per plant between the treatments with MOF compared with the control was statistically significant. The average weight of each fruit in the plants ranged from 15.12 to 28.01 kg; the highest in Treat.3 was 28.01 kg and the lowest in Treat.4 was only 15.12 kg. In comparison with the control, the average weight of each fruit in the experimental plants that were fertilized with MOF was higher, in which, the weight of the fruit in the treatment plants increased 12.89 kg (85.25% compared to the control). If this gourd variety was grown in Chach Trach village, My Tho commune of Phu My district, the average fruit weight was about 20-25 kg higher. The cause may be that the gravel soil in Hoai Huong ward, Hoai Nhon town was poor in nutrients and the weather conditions were not as favorable as in My Tho.

The application of MOF with suitable dosage has a positive influence on the growth and development of My Tho gourd, such as increasing chlorophyll, nitrogen and dry matter content, thereby increasing the length, diameter and thickness of fruit. In which, the best results were in Treat.3 with the application of 600 $kg.ha^{-1}$.

3.5.2. Theoretical and actual yield

The yield of gourd under the influence of MOF with different dosages is presented in Table 10.

Table 10. The yield of gourd

	Theoretical yield		Actual yield	
	$Ton.ha^{-1}$	% compare withcontrol	$Ton.ha^{-1}$	% compare withcontrol
CT1	156.17[c]	148.9	57.54[c]	186.0
CT2	200.69[b]	191.4	74.60[b]	241.2
CT3	307.99[a]	293.73	115.03[a]	371.9
CT4(DC)	104.86[d]	100	30.93[d]	100
CV (%)	**14.99**		**16.45**	
$LSD_{0.05}$	**10.54**		**4.76**	

Note: *Mean followed by the same letter isn't significantly different within the columns according to LSD test at a 5% significance level; CV: coefficient variance.*

https://doi.org/10.52111/qnjs.2022.16108

The theoretical yield of My Tho gourd in the treatments with microbial organic fertilizer was higher than that in the control without microbial organic fertilizer, ranging from 156.17 to 307.99 tons.ha^{-1}. The yield in Treat.3 was the highest (307.99 tons.ha^{-1}) and the lowest yield was in the control (104.86 tons.ha^{-1}). The actual yields of My Tho gourd were from 57.54 to 115.03 tons.ha^{-1}. In which, Treat.3 obtained the highest (115.03 tons.ha^{-1}) and Treat.4 obtained the lowest (57.54 tons.ha^{-1}). In comparison with the control, treatments 1, 2 and 3 with different dosages of microbial organic fertilizer increased 86.0%, 141.24% and 271.9 % respectively. There was a statistically significant difference between treatments with microbial organic fertilizer and with the control.

Thus, the addition of MOF increased the actual yield of My Tho gourd. This is similar to the results of many other studies on the effects of micro organic fertilizers for crop yield.[4,8,11,13]

Table 11. Economic efficiency of micro-organic fertilizer for gour

	Total income (1000 VND per ha)	Total cost (1000 VND per ha)	Profit (1000 VND per ha)	Profit ratio
Treat.1	73.710	34.260	39.450	1.15
Treat.2	103.320	34.810	68.510	1.96
Treat.3	174.300	35.360	138.940	3.92
Treat.4 (control)	40.670	32.060	8.610	0.27

The data from Table 11 shows that the highest profit was in Treat.3 (600 kg.ha^{-1}) which obtained 138,940 thousand VND, profit ratio reaching 3.92 times, followed by Treat.2 obtaining 68,510 thousand VND, and the lowest was in the control (8,610 thousand VND), with a profit ratio of 0.27.

4. CONCLUSION

The application of MOF on My Tho gourd plants at dosages of 400, 500, and 600 kg.ha^{-1} had a good effect on the chlorophyll content and dry matter content in leaves of My Tho gourd. The vitamin C content in the fruit increased from 0.2% to 5.29%, organic acid content increased from 13.97% to 40.53%, the dry matter mass increased from 0.15% to 1.48% and the Brix degree only increased from 0.09% - 1.2%. The average fruit weight increased from 6.08 to 12.89 kg, and the actual yield increased from 26.61 to 84.10 tons.ha^{-1} compared with the control. The highest efficiency was in treatment at dosage of 600 kg.ha-1 during the winter-spring crop 2020 - 2021 in Hoai Huong ward, Hoai Nhon town.

REFERENCES

1. Ministry of Health- Institute of Nutrition. *Table of nutritional ingredients of Vietnamese food,* Medicine Publishing house, Hanoi, 2000.
2. Doan Xuan Canh, Nguyen Duc Doan, Do Thi Thuy. Research on selection of lemon gourd varieties for the provinces of the RedRiver Delta, *Journal of Agricultural Science and Technology*, **2005**, *3*, 1-8.
3. Pham Thi Tran Chau, Nguyen Thi Hien and Phung Gia Tuong. *Biochemistry practice,* Education Publishing house, 2006.
4. Le Minh Chien. *Effect of microbial organic fertilizers on growth, yield and quality of cucumber,* Master thesis of Agricultural Science, Can Tho University, 2006.
5. Doan Cong Dien. Photosynthesis and dry matter accumulation of some sorghum varieties in arid conditions, *Journal of Science and Development,* **2013**, *11*(8), 1073-1080.
6. Le Van Khoa, Nguyen Xuan Cu, Bui Thi Ngoc Dung, Le Duc, Tran Khac Tiep, Cai Van Tranh. *Methods of analysis of soil, water, fertilizers, crops*, Education Publishing house, 2001.

7. Le Van Luy. *Report on the topic "Exploiting and developing Fiery Cross zucchini genetic resources in the South Central Coast",* Institute of Agricultural Science and Technology South Central Coast, 2012.

8. Vo Thi Hong Nhung. *Effect of microbial organic fertilizers on some growth, development and yield indicators of vegetable maize variety SG2 grown in An Nhon, Binh Dinh,* Master thesis in Experimental Biology, Quy Nhon University, 2013.

9. Dao Chau Thu. Effect of fertilizers on growth, development and yield of winter-spring crop, *Journal of Agricultural Science and Technology*, **2013**, *3*, 35-40.

10. Vo Minh Thu. Effect of microbial organic fertilizers on some yield and quality parameters of zucchini (Benincasa cerifera Savi), *Vietnam Journal of Agricultural Science and Technology*, **2016**, *8*(69), 50-54.

11. Vo Minh Thu, Nguyen Thi Y Thanh, Nguyen Tho Duc. Effect of microorganic fertilizers on some biochemical indicators, yield and quality of Korean gourd grown in Kon Tum*, Science Journal of Quy Nhon University*, **2019**, *5*(13), 95-101.

12. Nguyen Thi Van, Nguyen Ba Thong, Hoang Tuyet Minh. Study on the effect of dose of microbial organic fertilizer Song Gianh on growth, development and yield of rice variety VAAS 16 in Thanh Hoa, *Science Journal Vietnamese agricultural technology*, **2021**, *15*, 97-103.

13. Horst Marchner. *Mineral nutrition of higher plant*, Institute of plant University of Hohennerm Federal Republic of Germany, 1996.

14. Lincol Taizger. *Plant physiology,* 3 third edition, CRC, 2006.

https://doi.org/10.52111/qnjs.2022.16108

TẠP CHÍ KHOA HỌC
TRƯỜNG ĐẠI HỌC QUY NHƠN

Kỹ thuật ổn định và bù tần số cho thiết kế bộ khuếch đại thuật toán công suất thấp

Huỳnh Công Tú[1,*], Nguyễn Văn Hào[2], Huỳnh Nguyễn Bảo Phương[2]

[1]Phòng Đào tạo đại học, Trường Đại học Quy Nhơn, Việt Nam
[2]Khoa Kỹ thuật và Công nghệ, Trường Đại học Quy Nhơn, Việt Nam

Ngày nhận bài: 15/10/2021; Ngày nhận đăng: 15/11/2021

TÓM TẮT

Trong bài báo này, chúng tôi trình bày một thiết kế mạch khuếch đại thuật toán (op-amp) công suất thấp sử dụng các kỹ thuật bù Miller thông thường và bù Miller gián tiếp. Đối với op-amp hoạt động ở điện thế thấp, cách tiếp cận g_m/I_D được sử dụng để xác định kích thước bóng bán dẫn trong thiết kế mạch op-amp. Độ lợi, tốc độ tăng thế, biên độ pha, công suất tiêu tán và các thông số khác được xác định trong thiết kế. Để kiểm chứng các tham số của thiết kế, mạch op-amp được mô phỏng trên phần mềm LT-SPICE. Mục đích của nghiên cứu này là so sánh độ lợi và biên độ pha thu được khi sử dụng các kỹ thuật bù tần số khác nhau, từ đó xác định khả năng lựa chọn kỹ thuật bù tần số phù hợp dựa trên một tập hợp các yêu cầu thiết kế cụ thể. Trong nghiên cứu này, chúng tôi cũng sử dụng các ưu điểm khi kết hợp kỹ thuật bù phản hồi gián tiếp với bóng bán dẫn chia độ dài để thiết kế op-amp hiệu suất cao. Tất cả các thiết kế op-amp được thực hiện trên quy trình chế tạo CMOS 180 nanomet.

Từ khóa: *Khuếch đại thuật toán, công suất điện áp thấp, bù gián tiếp, khuếch đại thuật toán CMOS hai tầng.*

**Tác giả liên hệ chính.*
Email: huynhcongtu@qnu.edu.vn

JOURNAL OF SCIENCE
QUY NHON UNIVERSITY

Stability and frequency compensation techniques for low-power operational amplifier design

Huynh Cong Tu[1,*], Nguyen Van Hao[2], Huynh Nguyen Bao Phuong[2]

[1]Undergraduate Training Office, Quy Nhon University, Vietnam
[2]Faculty of Engineering and Technology, Quy Nhon University, Vietnam

Received: 15/10/2021; Accepted: 15/11/2021

ABSTRACT

A low-power operational amplifier (op-amp) circuit with both conventional and indirect Miller compensating techniques is presented in this work. For low-voltage op-amps, the g_m/I_D method is used to calculate transistor size. The gain, slew rate, phase margin, power dissipation, and other parameters of the proposed op-amp were determined. The developed op-amp circuit was simulated in LT-SPICE to check parameter values. The goal of this study was to examine the gain and phase margins obtained using several frequency compensation techniques in order to identify the best one for a given set of design requirements. To create a high performance op-amp, we used split-length transistors combined with indirect feedback compensation. All op-amps were designed in 180 nm CMOS technology.

Keywords: *Op-amp, Low-voltage low-power, Indirect compensation, Two stage CMOS operational amplifier.*

1. INTRODUCTION

The operational amplifier (op-amp) is a very versatile analog circuit that is frequently used in analog and mixed-signal Integrated Circuit (IC) design.[1,2] Op-amps are frequently developed using sub-micron Complementary Metal Oxide Semiconductor (CMOS) technology, for example, nodes 350 nm, 180 nm, and 130 nm. However, there are numerous approaches for designing the op-amp to meet the requirements of various circuits.[3,4] It typically consists of two or more amplification stages that utilize transistors, integrated capacitors, and, in some cases, integrated resistors. All op-amps, however, must have enough open-loop margin of stability in order to be used in a feedback closed-loop design with acceptable frequency response. As a result, the open-loop configuration of an op-amp should have a phase margin (PM) of 45° or greater, which can be accomplished by the use of Miller compensating techniques. To obtain the required stability and frequency responsiveness, many compensating strategies may be used. These compensation strategies may be used singly or in combination.[3]

Frequency compensation is critical for close-loop stability when designing the op-amps that operate the negative feedback connection. Miller compensation is one of the techniques used to enhance the op-amp's stability and frequency response.[5] The Miller effect can be detected in two ways within a MOSFET analog amplifier. To begin, the Miller effect is created by the MOSFET's construction, which has five

**Corresponding author.*
Email: huynhcongtu@qnu.edu.vn

https://doi.org/10.52111/qnjs.2022.16109

capacitances between its terminals: drain (D), gate (G), source (S), and bulk (B), as illustrated in Figure1. The capacitance difference between the drain and gate terminals (C_{GD}) establishes a feedback connection between the drain and gate terminals. While C_{GD} is often a low capacitance value, it also demonstrates the effect of the amplifier's high-frequency response. Miller capacitance is the name given to the capacitance C_{GD}.[5]

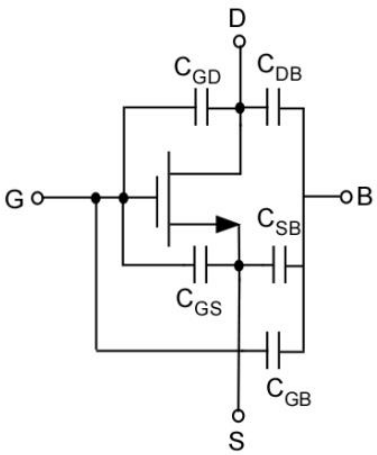

Figure 1. Parasitic capacitances in MOSFET

Second, it can be accomplished by adding an external capacitor (C_c) to the second stage of a standard two-stage CMOS op-amp, as illustrated in Figure 2. A connection between the second stage and the external Miller capacitor (C_c) may be seen in this diagram.

The frequency compensation technique will be demonstrated in this study for the design of operational amplifiers. The direct Miller compensation technique is used in the first design. When comparing the two designs, the indirect Miller compensating technique in conjunction with a split-length transistor is employed in the second design.

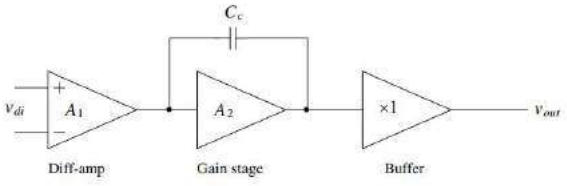

Figure 2. Block diagram of the second voltage amplifier stage with Miller compensation.

Additionally, the Nulling Resistor approach is employed in both designs to boost the efficiency of the operational amplifier. The target amplifier is a two-stage CMOS operational amplifier (op-amp) that operates on a +0.9 V power supply and has high unity gain as well as stability. All simulation investigations were also carried out using the LT-SPICE circuit simulator, which may be found here.

2. DESIGN OF TWO-STAGE OPERATIONAL AMPLIFIER WITH MILLER COMPENSATION

2.1. Design of two stages operational amplifier

Because of its simple structure and robustness, the two-stage CMOS operational amplifier is widely utilized. It also has a high DC gain as well as a wide range of output voltage swings. Transistor M1 and M2 together constitute a differential amplifier, which converts differential voltage to current in the first stage of a two-stage operational amplifier design (Figure 3). This differential current is then sent to the current mirror circuit, which is formed by M3 and M4, which recovers the voltage difference between the two stages. The output of the first stage operational amplifier is essentially identical to the output of the differential voltage amplifier. The M6 is responsible for supplying the differential pair with the bias current I_{B1}. The second stage is comprised of a common source MOSFET amplifier M7, which converts the input voltage of the second stage into current through the use of a MOSFET transistor. The common source transistor is actively loaded with the current sink load M8, which turns the current back into a voltage at the output of the transistor at the same time. Transistor M8 does not provide biasing for transistor M7, and M7 is biased from the gate side of the transistor M8. As a result, the second stage functions similarly to a current sink inverter.

2.2. Miller Compensation

An external Miller capacitor is commonly connected between the output of the second stage and the output of the first stage transistors, as shown in Figure 2.

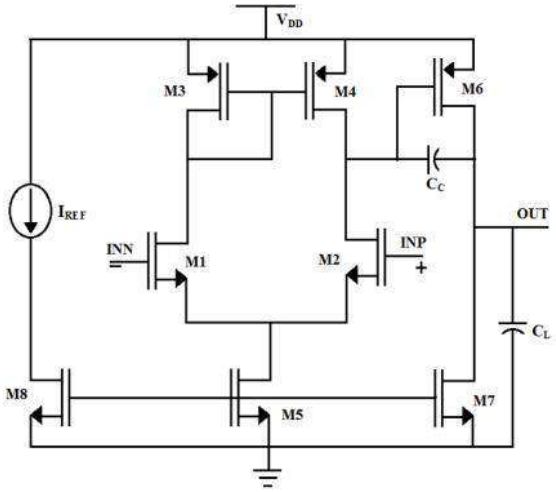

Figure 3. Miller compensated two stage operational amplifier

Figure 4 presents the small-signal model of the two-stage amplifier illustrated in Figure 3, which does not include compensation. When the operational amplifier gain is expressed as a two-pole open-loop transfer function, the result is as follows:[9]

$$\frac{V_{out}}{V_{in}} = A(s) = \frac{A_V}{\left(1+\frac{s}{p_1}\right)\left(1+\frac{s}{p_2}\right)} \quad (1)$$

Where V_{in} represents a small signal differential input voltage. A_V is the op-amp gain and poles p_1 and p_2 are defined by the capacitances linked to the high impedance of the op-amp. In addition, the small-signal equivalent circuit of the two-stage amplifier is shown in Figure 4 when $p_2 >> p_1$, which implies p_1 is the dominant pole. And the small-signal analysis is presented by:

$$A_V = G_{m1}G_{m2}R_1R_2, p_1 = \frac{G_{m1}}{C_1}, p_2 = \frac{G_{m2}}{C_L}$$

A feedback path for an op-amp is provided by the linked Miller capacitor. The transfer function equation at node V_{in} has an effect on the capacitor C_c, resulting in the following [9]:

$$\frac{V_{out}}{V_{in}} = \frac{R_2R_1G_{m1}G_{m2}\left(1-\frac{sC_c}{G_{m2}}\right)}{\left[\begin{array}{c}1+s\left(C_1R_1+C_2R_2+C_c(R_1+G_{m2}R_1R_2+R_2)\right)\\+s^2R_1R_2(C_cC_2+C_cC_1+C_1C_2)\end{array}\right]} \quad (2)$$

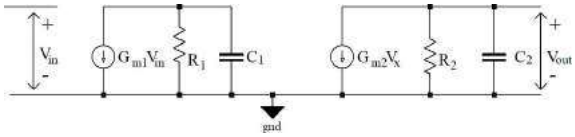

Figure 4. Small-signal model op-amp without compensation

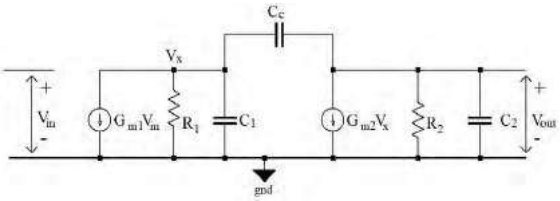

Figure 5. Small-signal model op-amp with compensation

The ratio $V_{out}/V_{in} = G_{m1}R_1G_{m2}R_2$ if s=0. If $s \neq 0$, the Miller effect in the right half plane causes zero transmission in the op-amp:

$$1 - \frac{sC_c}{G_{m2}} = 0, p_z = s_z = \frac{G_{m2}}{C_c}$$

The denominator polynomial for an op-amp with two poles is:

$$Y(s) = \left(1+\frac{s}{p_1}\right)\left(1+\frac{s}{p_2}\right) = 1 + s\left(\frac{1}{p_1}+\frac{1}{p_2}\right) + s^2\left(\frac{1}{p_1p_2}\right) \quad (3)$$

If there is one dominant pole, $p_1 << p_2$ and Y(s) can be:

$$Y(s) = 1 + s\left(\frac{1}{p_1}\right) + s^2\left(\frac{1}{p_1p_2}\right) \quad (4)$$

Finding the frequency of the first dominant pole can be done by equating the first and second dominant poles together.

$$p_1 = \frac{1}{R_1C_1 + R_2C_2 + C_c(G_{m2}R_1R_2 + R_1 + R_2)} \quad (5)$$

The term $(C_c(G_{m2}\ R_1R_2+R_2+R_1))$ can be realised by connecting it to the first and second stages where C_c is the negative feedback path of the second stage. Moreover, the first term (R_1C_1) is much larger than the second term (R_2C_2) and, usually, C_1 is much smaller than the Miller capacitance. The approximate value of the p_1 is:

$$p_1 = \frac{1}{C_cG_{m2}R_1R_2} \quad (6)$$

The non-dominant pole as the frequency of the second pole can be found by equating:

https://doi.org/10.52111/qnjs.2022.16109

$$p_2 = \frac{C_c G_{m2} R_1 R_2}{R_1 R_2 (C_1 C_2 + C_1 C_c + C_2 C_c)} \quad (7)$$

Meanwhile, $C_1 << C_2$ and $C_1 << C_c$, the approximation of the p_2 can be shown as:

$$p_2 = \frac{G_{m2}}{C_2} \quad (8)$$

The unity gain frequency (UGF) of the two-stage amplifier is given by:

$$UGF = \frac{G_{m1}}{C_c} \quad (9)$$

The location of the zero set in the right half-plane in the transfer function and the location of pole-zero is described in Figure 6, (where jw is the imaginary axis and σ is the real axis), it creates a negative phase shift of the amplifier.[5] To achieve the closed-loop gain stability, the location of p_2 and p_z must be at higher frequencies than UGF. If C_c is increased the UGF reduces to approach the stability condition, PM >> 60° and p_2 is located at half of UGF.[3] Moreover, as C_c is increased, p_1 is decreased, and it permits to move p_z further to the right half-plane and p_2 to higher frequencies.

It is shown in Figure 6 that by placing the zero set in the right half-plane of the transfer function and the placement of pole-zero (where jω is the imaginary axis and is the real axis), a negative phase shift is created in amplifier.[5] In order to achieve closed-loop gain stability, the locations of p_2 and p_z must be at frequencies higher than those of the UGF. The UGF decreases until it approaches the stability condition, PM > 60°, and p_2 is positioned at half of the UGF when C_c is increased. Furthermore, as C_c is increased, p_1 decreases, allowing for the displacement of p_z farther to the right half-plane and the expansion of p_2 to higher frequencies.

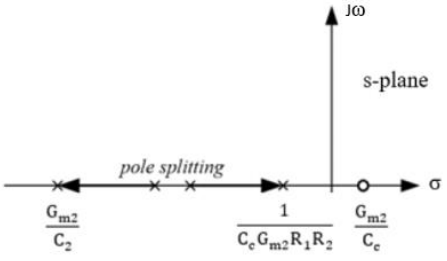

Figure 6. Pole/zero locations

2.3. Procedure of a conventional op-amp design

The conventional design for an operational transconductance amplifier (shown in Figure 3) is based on the large-signal and small-signal device modeling equations when the transistors are operated within the saturation region for power supply of ±0.9 V. The transistor takes after certain conditions, which are called the DC balance conditions as follows:

1. For PM greater than 60°, the second pole (p_2) (or output pole) is considered more significant than 2.2 UGF.

2. First zero is much higher than the second pole, therefore, $p_2 \geq 2.2$ UGF and $z \geq 10$UGF.

3. Assume that $V_{SG4} = V_{SG6}$, this causes "proper mirroring" in the M3-M4 mirror. Furthermore, the gate and drain terminals of the transistor M3 are at the same potential so that transistor M4 is in saturation.

4. Calculate the current for each transistor I_4,I_5,I_6,I_7 according to the square root of drain current (saturation region)[9]

$$\text{If } V_{SG4} = V_{SG6} \qquad I_6 = \frac{W_6}{W_4} I_4 \quad (10)$$

5. When V_{SG5}=V_{SG7}

$$I_7 = \frac{W_7}{W_5} I_5 = \frac{W_7}{W_5} 2I_4 \quad (11)$$

6. For balance, I_6 must equal I_7. This condition is called the "balance conditions".

$$\frac{W_6}{W_4} = \frac{2W_7}{W_5} \quad (12)$$

The op-amp has been designed to operate with a 0.9 V supply. The operational amplifier is designed using the strong inversion region. The transistor dimensions are calculated using the saturation region equation and represent the width and length of each transistor.

3. CALCULATION AND SIMULATION RESULTS

The design parameters of an op-amp with its specifications are given in table 1:

Table 1. The design goal of the operational amplifier

Parameters	Specification
Gain	60dB
Power supply V_{DD}	0.9 V
Gain Bandwidth (GB)	5MHz
Load capacitance C_L	10pF
Slew rate (SR)	10V/μs
Phase margin (PM)	>55°
Input Common Mode Range (ICMR)	0.4V to 0.9V
Power Dissipation	≤ 1mW

We may utilize MOSFETs as small as 180 nm in length (L) and 400 nm in width (W) with the 180 nm technology, but due to the rise in the channel length modulation (λ), we normally do not employ the minimal channel length. It is recommended to utilize $L > 2L_{min}$. Nonetheless, the device length (L) is set to 1 μm in this design and is used throughout the circuit. This value is used to calculate the channel length modulation parameter, which is necessary to calculate the amplifier gain. Following that, to optimize the op-amp's performance, we'll adjust the length of selected MOSFETs while maintaining a constant (W/L). For the calculations, we will use the MOSFET transconductance parameters k_n = 170 $\mu A/V^2$ (for nMOS) and k_p = 36 $\mu A/V^2$ (for pMOS) as input parameters. The saturated drain current i_D in MOSFET is given by:

For nMOS

$$i_D = \frac{1}{2} k_n \frac{W}{L} (v_{GS} - V_T)^2 (1 + \lambda) \qquad (13)$$

For pMOS

$$i_D = \frac{1}{2} k_p \frac{W}{L} (v_{GS} - V_T)^2 (1 + \lambda) \qquad (14)$$

Where λ is channel length modulation. We use λ = 0.05 V^{-1} for pMOS and for λ = 0.04 V^{-1} nMOS in the calculation.

Calculate the value of the compensation capacitor C_c after determining the device length.

$$C_c > \frac{2.2}{10} C_L = 2.2pF$$

C_c were selected as 3pF.

Next, based on the slew rate requirements, determine the minimum value of tail current I_5. The formula used to compute the value of I_5 is.

$$I_5 = \text{SR}.C_c = (3.10^{-12})(10.10^6) = 30\ \mu A$$

Determine the aspect ratio of M3 by following relation, where the threshold voltage is denoted by V_T. Calculate sensitivity S_3 using the equation:

$$S_3 = (W/L)_3 = \frac{I_5}{k_p[V_{DD} - V_{in}(max) - |V_{T0}|_{(max)} + V_{T1(min)}]^2} \geq 1$$

$$= \frac{30.10^{-6}}{(36.10^{-6})[0.9 - 0.5 - 0.85 + 0.55]^2} = 83$$

Since, M3 and M4 are identical S_3 will be equal to S_4.

$$(W/L)_3 = (W/L)_4 = 83$$

The equation that follows determines the input transistor's transconductance:

$$g_{m1} = GB.C_c.2\pi = (5.10^6)(2\pi)(3.10^{-12}) = 94.25\ \mu s$$

From the above equation, the aspect ratio of M1 and M2 can be directly obtained as:

$$(W/L)_1 = (W/L)_2 = \frac{g_{m1}^2}{k_n I_5} = \frac{(94.25\mu)^2}{(170.10^{-6})(30.10^{-6})} = 1.74 \sim 2$$

The aspect ratio S_5 and S_6 is determined as:

$$S_5 = (W/L)_5 = \frac{2I_5}{k_n[V_{DS5(sat)}]^2}$$

$$V_{DS5(\text{sat})} = V_{\text{in}\,(min)} - V_{SS} - \sqrt{\frac{I_5}{\beta_1}} - V_{T1(max)} \geq 100\text{mV}$$

$$V_{DS5(sat)} = -0.1 + 0.9 - \sqrt{\frac{30.10^{-6}}{170.10^{-6}.3}} - 0.3 = 0.26\ \text{V}$$

$$S_5 = (W/L)_5 = \frac{2I_5}{k_n[V_{DS5(sat)}]^2} = \frac{2\,(30.10^{-6})}{170.10^{-6}[0.26]^2} = 5.2$$

$S_6 = S_4 \frac{g_{m6}}{g_{m4}}$ with condition $g_{m6} \geq 10 g_{m1} \geq 942.5\mu s$

$$S_6 = S_4 \frac{g_{m6}}{g_{m4}} = 60 \frac{942.5\mu}{300\mu} = 188.5$$

https://doi.org/10.52111/qnjs.2022.16109

The following equation can be used to calculate the current via M6.

$$I_6 = \frac{g_{m6}^2}{2k_p S_6} = \frac{(942.5\mu)^2}{2(30.10^{-6})(188.5)} = 78.54\mu\text{A}$$

S_7 should be designed in such a way that the desired current ratios between I_5 and I_6 are achieved:

$$(W/L)_7 = \frac{I_6}{I_5} S_5 = 2.2\frac{78.54\mu}{30\mu} = 5.76$$

Finally determine the value of gain and power dissipation and check its specification.

$$\begin{aligned} P_{\text{diss}} &= (I_5 + I_6)(V_{DD} + |V_{SS}|) \\ &= (30\mu + 78.54\mu)(0.9 + 0.9) \\ &= 0.000195 = 195\ \mu W \end{aligned}$$

To determine A_V

$$\begin{aligned} A_V &= 2\frac{g_{m2}g_{m6}}{I_5(\lambda_2 + \lambda_3)I_6(\lambda_6 + \lambda_7)} \\ &= 2\frac{(94.25\mu)(942.5\mu)}{30.10^{-6}(0.04 + 0.05)78.54.10^{-6}(0.04 + 0.05)} \\ &= \frac{9308.83\text{V}}{\text{V}} = 79.8\ dB \end{aligned}$$

All simulations were conducted using typical model process transistor models and the LT-Spice circuit simulator to verify that all design parameters were met, including unity gain frequency (UGF), phase margin (PM), and DC gain.

The results of aspect ratio of each transistor are summarized in Table 2.

Figure 7 illustrates the results of the first op-amp design when various Miller capacitor values are used. As a result of increasing the Miller compensation (increasing the value of C_c), the phase margin has increased, while the unity gain frequency has reduced. In transfer function, the compensation capacitor yields a right-half plane zero.[8] It results in a phase shift toward the negative. The zero-nulling resistor has been used to eliminate this effect (Figure 8).

Table 2. Aspect ratio of each transistor

Transistor	W(µm)	L(µm)	W/L
M_1, M_2	2	1	2
M_3, M_4	83	1	83
M_5	5.2	1	5.2
M_6	188.5	1	188.5
M_7	5.76	1	5.76

The outcome demonstrates a well-behaved step reaction. When the zero is shifted to the left-half plane (LHP), the zero's phase response is added to the total phase response, thereby increasing the phase margin.

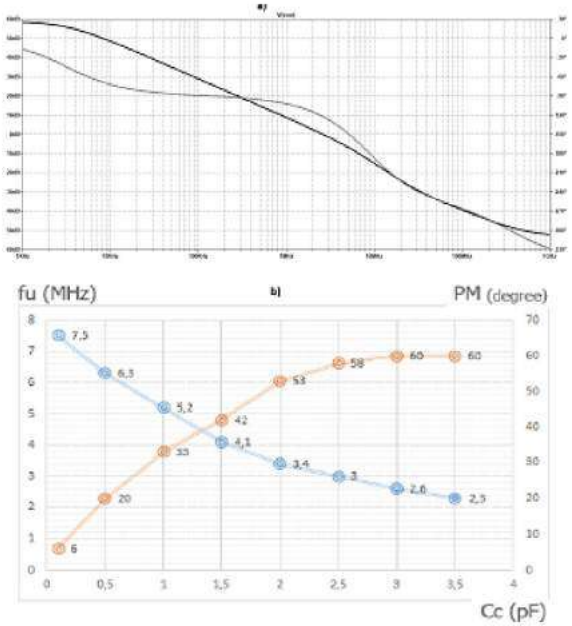

Figure 7. Results for the first op-amp design. a) frequency response of the first op-amp. b) Unity gain frequency and phase margin with different miller capacitor values.

Indirect Miller compensating techniques are used in the second op-amp design. Indirect compensation of the op-amp can be accomplished by cascading the internal low impedance nodes. This node can be built by utilizing the proposed split-length transistor in work.[6]

Figure 9 illustrates the recommended architecture in this article. To prevent the RHP zero, the addition of MOSFETs results in the formation of a common-gate amplifier. The

current I_{Cc} is sent back to the differential op-amp's output via the common-gate MOSFET. Figure 10 illustrates the result of the opamp simulation utilizing the indirect compensation strategy demonstrated in Figure 9.

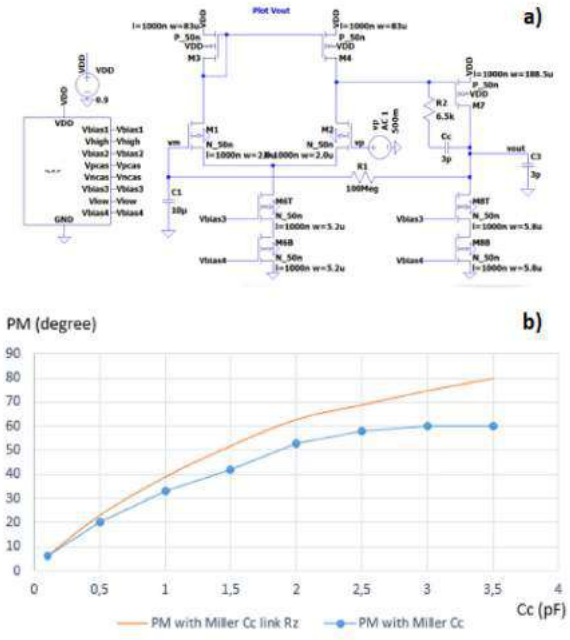

Figure 8. Two-stage op-amp employing miller capacitor and nulling resistor (a) and phase margin with different miller capacitor values (b).

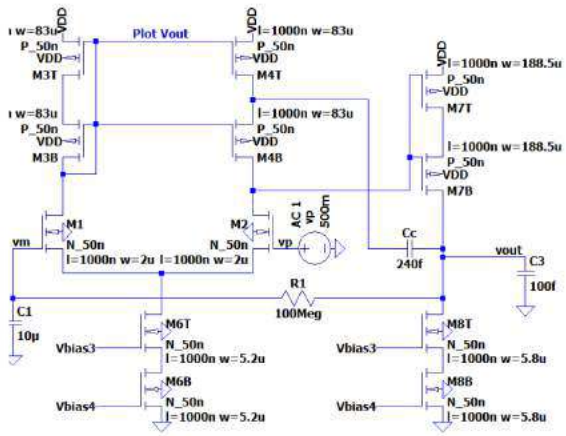

Figure 9. Two-stages op-amp design using Indirect Compensation technique and the split-length transistor.

Because indirect Miller eliminates the initial zero in addition to separating the poles, it speeds up op-amp circuits, adjusts phase margin, and improves UGF.

A comparison of the two operational amplifier designs is shown in Table 3. The DC gain, common mode rejection ratio (CMRR), and power supply rejection ratio (PSRR) have remained constant due to the fact that the input differential pair or current summing branches do not contribute to the PSRR. The UGF is related to power dissipation. The UGF increases with increasing power dissipation. When compared to the previously published work,[7] the power dissipation of the developed operational amplifiers is reduced (Table 3).

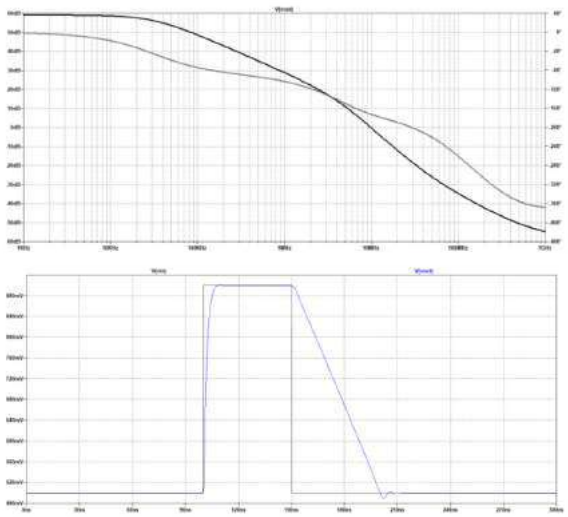

Figure 10. Frequency response and slew rate of op-amp using the indirect compensation with a compensation capacitor of 240 fF.

Table 3. Summary of op-amp simulations

Performance	Reported work [7]	First op-amp	Second op-amp
Power supply (V)	5.0	+0.9	+0.9
Process (µm)	0.35	0.18	0.18
DC gain (dB)	77.25	59	60.2
UGF (MHz)	8.6	2.6	5.7
PM (degree)	53.46	60	57.3
SR (V/µs)	10.4	4.8	7.5
Settling time (ns)	400	234	186
CL (pF)	10	3	3
VOH (V)	3.28	1.2	1.2
VOL (mV)	0	0.2	0.2
ICMR	0.9-3.27	0-1.2	0-1.2
Power dissipation (µW)	480	195	152

https://doi.org/10.52111/qnjs.2022.16109

4. CONCLUSION

The paper discusses two op-amp designs with varied gain frequencies and phase margins. Miller (direct) compensation was used to improve the PM; however, the poles were split and a RHP zero was included, resulting in a decrease in the UGF. Additionally, by utilizing split-length transistors for indirect compensation, the PM was corrected and the UGF was enhanced. This design results in a significant increase in the unity gain frequency while keeping an acceptable phase margin, increasing the op-amp's speed and stability.

Acknowledgement

This research is conducted within the framework of science and technology projects at institutional level of Quy Nhon University under the project code T2020.669.17.

REFERENCES

1. K. Lundager, B. Zeinali, M. Tohidi, J. K. Madsen, and F. Moradi. Low power design for future wearable and implantable devices, *Journal of Low Power Electronics and Applications*, **2016**, 6, *4*, 97-102.
2. A.L.S. Loke et al., *Analog/Mixed-Signal Design in FinFET Technologies,* in *Hybrid ADCs, Smart Sensors for the IoT, and Sub-1V & Advanced Node Analog Circuit Design*, Springer International Publishing, 2018, 259–280.
3. Baker, R.J. *CMOS Circuit Design, Layout, and Simulation*, Fourth Edition, John Wiley & Sons, 2019.
4. Z. Qin, A. Tanaka, N. Takaya, and H. Yoshizawa. 0.5-V 70-nW Rail-to-Rail Operational Amplifier Using a Cross-Coupled Output Stage, *IEEE Transactions on Circuits and Systems II:* Express Briefs, **2016**, *63*(11),1009-1013.
5. Eschauzier, Rudy G.H., Huijsing, Johan. Frequency Compensation Techniques for Low-Power Operational Amplifiers, *The Springer International Series in Engineering and Computer Science*, **1995**, 313.
6. V. Saxena and R. Baker. Indirect Compensation Techniques for Three-Stage Fully-Differential Op-Amps, *53rd IEEE International Midwest Symposium on Circuits and Systems*, **2010**, 588-591.
7. Shruti Suman. Two Stage CMOS Operational Amplifier: Analysis and Design, *Mody University International Journal of Computing and Engineering Research,* **2019**, *3*(1), 40-44.
8. Abolfazl Sadeqi1, Javad Rahmani et al. Design method for two-Stage CMOS operational amplifier applying load/miller capacitor compensation, *Computational Research Progress in Applied Science & Engineering*, **2020,** *06*(03), 153-162.
9. Razavi, Behzad. *Design of analog CMOS integrated circuits, MC GRAW HILL INDIA*, 2017.

TẠP CHÍ KHOA HỌC
TRƯỜNG ĐẠI HỌC QUY NHƠN

Phép chiếu Bergman tác động lên L^∞ trên hình cầu đơn vị $\mathbb{B}_n$

Lê Văn An*

Khoa Toán và Thống kê, Trường Đại học Quy Nhơn, Việt Nam.

Ngày nhận bài: 31/10/2021, Ngày nhận đăng: 24/12/2021

TÓM TẮT

Với một hàm trọng cho trước, ta định nghĩa phép chiếu kiểu Bergman cảm sinh bởi hàm trọng đó. Chúng tôi đưa ra một đặc trưng của hàm trọng bán kính để phép chiếu kiểu Bergman đó là bị chặn từ L^∞ vào không gian Bloch $\mathcal{B}$ trên hình cầu đơn vị $\mathbb{B}_n$ của $\mathbb{C}^n, n > 1$.

Từ khóa: *Không gian Bergman, phép chiếu Bergman, không gian Bloch.*

**Tác giả liên hệ chính.*
Email: levanan@qnu.edu.vn

https://doi.org/10.52111/qnjs.2022.16110

JOURNAL OF SCIENCE
QUY NHON UNIVERSITY

On the Bergman projections acting on L^∞ on the unit ball $\mathbb{B}_n$

Van An Le*

Department of Mathematics and Statistics, Quy Nhon University, Vietnam.

Received: 31/10/2021; Accepted: 24/12/2021

ABSTRACT

Given a weight function, we define the Bergman type projection induced by this weight. We characterize the radial weights such that this projection is bounded from L^∞ to the Bloch space $\mathcal{B}$ on the unit ball $\mathbb{B}_n$ of $\mathbb{C}^n, n > 1$.

Keywords: *Bergman space, Bergman projection, Bloch space.*

1. INTRODUCTION AND MAIN RESULT

Let $\mathbb{C}^n$ denote the n-dimensional complex Euclidean space. For any two points $z = (z_1, \dots, z_2)$, $w = (w_1, \dots, w_n)$ in $\mathbb{C}^n$, we use the well-known notation

$$\langle z, w\rangle = z_1\overline{w_1} + \cdots + z_n\overline{w_n},$$

and $|z| = \sqrt{\langle z, z\rangle}$.

Let $\mathbb{B}_n = \{z \in \mathbb{C}^n : |z| < 1\}$ be the unit ball, and let $\mathbb{S}_n = \{z \in \mathbb{C}^n : |z| = 1\}$ be the unit sphere in $\mathbb{C}^n$.

Denote by $H(\mathbb{B}_n)$ the space of all holomorphic functions on the unit ball $\mathbb{B}_n$. Let dv be the normalized volume measure on $\mathbb{B}_n$. The normalized surface measure on $\mathbb{S}_n$ will be denoted by $d\sigma$.

Let ρ be a positive and integrable function on $[0, 1)$. We extend it to $\mathbb{B}_n$ by $\rho(z) = \rho(|z|)$, and call such ρ a radial weight function. The weighted Bergman space A^2_ρ is the space of functions f in $H(\mathbb{B}_n)$ such that

$$\|f\|^2_\rho = \int_{\mathbb{B}_n} \big|f(z)\big|^2 \rho(z)dv(z) < \infty.$$

Let ρ be a radial weight and X be a space of measurable functions on $\mathbb{B}_n$. The Bergman type projection P_ρ acting on X is given by

$$P_\rho f(z) = \int_{\mathbb{B}_n} K_\rho(z, w)f(w)\rho(w)dv(w),$$

for $z \in \mathbb{B}_n, f \in X$, where $K_\rho(z, w)$ is the reproducing kernel of the weighted Bergman space A^2_ρ.

When ρ is the standard radial weight $\rho(z) = (1-|z|^2)^\alpha, \alpha > -1$, the corresponding projection is denoted by P_α.

Corresponding author.
Email: levanan@qnu.edu.vn

https://doi.org/10.52111/qnjs.2022.16110

A radial weight ρ belongs to the class $\widehat{\mathcal{D}}$ if $\widehat{\rho}(r) \lesssim \widehat{\rho}(\frac{1+r}{2})$ for all $r \in [0,1)$, where $\widehat{\rho}(r) = \int_r^1 \rho(s)ds$.

The Bergman space and a lot of topics related to this famous space have attracted the attention of many mathematicians so far. When the weight function is the standard radial weight, the theory of Bergman space is well-known. We recommend the books of Zhu[9,10] for more details.

In 2018, we began the study of small Bergman spaces in higher dimensions[5]. The projections play a crucial role in studying operator theory on spaces of analytic functions. Bounded analytic projections can also be used to establish duality relations and to obtain useful equivalent norms in spaces of analytic functions. Hence the boundedness of projections is an interesting topic which has been studied by many authors in recent years[1,2,3,7,8]. In[7], Peláez and Rättyä considered the projection P_{ρ_1} acting on $L^p_{\rho_2}(\mathbb{D}), 1 \leq p < \infty$, when two weights ρ_1, ρ_2 are in the class $\mathcal{R}$ of the so called regular weights. A radial weight ρ is regular if $\widehat{\rho}(r) \asymp (1-r)\rho(r), r \in (0,1)$. Recently, in 2019, they extended these results to the case where $\rho_1 \in \widehat{\mathcal{D}}$, ρ_2 is radial[8].

In this paper, we are going to study the projections acting on the space L^∞. Let us recall that the Bloch space of $\mathbb{B}_n$, denoted by $\mathcal{B}(\mathbb{B}_n)$, or simply by $\mathcal{B}$, is the space of holomorphic functions f on $\mathbb{B}_n$ such that

$$\sup_{z\in\mathbb{B}_n}(1-|z|^2)\big|Rf(z)\big| < \infty,$$

where

$$Rf(z) = \sum_{j=1}^n z_j \frac{\partial f}{\partial z_j}(z)$$

is the radial derivative of f at $z \in \mathbb{B}_n$. In the one dimensional case, the Bloch space consists of analytic functions f on $\mathbb{D}$ such that

$$\sup_{z\in\mathbb{D}}(1-|z|^2)\big|f'(z)\big| < \infty,$$

and is denoted by $\mathcal{B}(\mathbb{D})$.

In the case of standard radial weight, we have the following result.

Theorem A. *For any $\alpha > -1$, the Bergman type projection P_α is a bounded linear operator from L^∞ onto the Bloch space $\mathcal{B}$.*

This theorem is also valid for the case of one dimension $\mathbb{C}$ and of higher dimension $\mathbb{C}^n$. See[10] Theorem 5.2 for the proof in the case of one variable and[9] Theorem 3.4 for the proof in the case of several variables.

When the weight functions is more general, in[8], Peláez and Rättyä obtained an interesting result in the one dimensional case.

Theorem B. *Let ρ be a radial weight. Then the projection $P_\rho : L^\infty(\mathbb{D}) \to \mathcal{B}(\mathbb{D})$ is bounded if and only if $\rho \in \widehat{\mathcal{D}}$.*

The aim of this paper is to study the Bergman type projections acting on L^∞ in the case of higher dimension. In this case, what will be the target space and the characterizations of the weight functions such that the projection is bounded? We extend Theorem B to the case of several variables and obtain the following result.

Theorem 1.1. *Let ρ be a radial weight. Then the projection $P_\rho : L^\infty \to \mathcal{B}$ is bounded if and only if $\rho \in \widehat{\mathcal{D}}$.*

The paper is organized as follows. In Section 2, we give some important lemmas which are used in the proof of Theorem 1.1 and Section 3 gives us an explicit explanation for our main result.

Throughout this text, the notation $U(z) \lesssim V(z)$ (or equivalently $V(z) \gtrsim U(z)$) means that there is a positive constant C such that $U(z) \leq C.V(z)$ holds for all z in

https://doi.org/10.52111/qnjs.2022.16110

the set in question, which may be a space of functions or a set of numbers. If both $U(z) \lesssim V(z)$ and $V(z) \lesssim U(z)$ hold, then we write $U(z) \asymp V(z)$.

2. SOME AUXILIARY LEMMAS

To prove Theorem 1.1 we need several auxiliary lemmas.

Lemma 2.1. *Let ρ be a radial weight. Then the following conditions are equivalent:*

(i) $\rho \in \widehat{\mathcal{D}}$;

(ii) There exist $C = C(\rho) > 0$ and $\beta_0 = \beta_0(\rho) > 0$ such that

$$\widehat{\rho}(r) \leq C \left(\frac{1-r}{1-t}\right)^{\beta} \widehat{\rho}(t),$$

where $0 \leq r \leq t < 1$, for all $\beta \geq \beta_0$;

(iii) The asymptotic equality

$$\int_0^1 s^x \rho(s) ds \asymp \widehat{\rho}\left(1 - \frac{1}{x}\right),$$

where $x \in [1, \infty)$, is valid;

(iv) There exist $C_0 = C_0(\rho) > 0$ and $C = C(\rho) > 0$ such that

$$\widehat{\rho}(0) \leq C_0 \widehat{\rho}(\frac{1}{2})$$

and $\rho_n \leq C\rho_{2n}$ for all $n \in \mathbb{N}$.

Lemma 2.1 gives us the characterizations of the weight function $\rho \in \widehat{\mathcal{D}}$. The proof of this lemma can be found in[6].

Lemma 2.2. *If*

$$f(z) = \sum_{n=0}^{\infty} a_j z^j \in H^p, \qquad 0 < p \leq 2,$$

where H^p denotes the Hardy space, then

$$\sum_{j=0}^{\infty} (j+1)^{p-2} \left|a_j\right|^p \lesssim \|f\|_p^p.$$

Lemma 2.3. *Let $\{a_j\}$ be a sequence of complex numbers such that $\sum j^{q-2} \left|a_j\right|^q < \infty$ for some $q, 2 \leq q < \infty$. Then the function $f(z) = \sum_{n=0}^{\infty} a_j z^j$ is in H^q, and*

$$\|f\|_q^q \lesssim \sum_{j=0}^{\infty} (j+1)^{q-2} \left|a_j\right|^q.$$

Two above lemmas are the classical Hardy-Littlewood inequalities, which can be found, for example, in Duren's book[4] Theorem 6.2 and 6.3.

In the following lemma, we give the explicit formula for the reproducing kernel of A^2_ρ.

Lemma 2.4. *Let ρ be a radial weight. Then the reproducing kernel $K_\rho(z, w)$ is given by*

$$K_\rho(z, w) = \frac{1}{2} \sum_{d=0}^{\infty} \frac{(d+n-1)!}{d!n!\rho_{2n-1+2d}} \langle z, w\rangle^d,$$

for $z, w \in \mathbb{B}_n$, where

$$\rho_x = \int_0^1 t^x \rho(t) dt, \qquad x \geq 1.$$

Proof. By the multinomial formula (see[9] (1.1)), we have that

$$\langle z, w\rangle^d = \sum_{\beta \in \mathbb{N}^n, |\beta| = d} \frac{d!}{\beta!} z^\beta \bar{w}^\beta, \qquad z, w \in \mathbb{C}^n,$$

where $|\beta| = \beta_1 + \cdots + \beta_n, \beta! = \beta_1! \ldots \beta_n!$ for each $\beta = (\beta_1, \ldots, \beta_n) \in \mathbb{N}^n$. Hence, for $\alpha \in \mathbb{N}^n, |\alpha| = d$,

$$\int_{\mathbb{S}_n} \xi^\alpha \langle z, \xi\rangle^d d\sigma(\xi) = \sum_{\beta \in \mathbb{N}^n, |\beta| = d} \frac{d! z^\beta}{\beta!} \int_{\mathbb{S}_n} \xi^\alpha \bar{\xi}^\beta d\sigma(\xi),$$

where $z \in \mathbb{B}_n$. By Lemma 1.11 in[9],

$$\int_{\mathbb{S}_n} \xi^\alpha \bar{\xi}^\beta d\sigma(\xi) = \begin{cases} 0 & \text{if } \alpha \neq \beta, \\ \dfrac{\alpha!(n-1)!}{(d+n-1)!} & \text{if } \alpha = \beta, \end{cases}$$

https://doi.org/10.52111/qnjs.2022.16110

and we obtain

$$\int_{\mathbb{S}_n} \xi^\alpha \langle z,\xi\rangle^d d\sigma(\xi) = \frac{d!}{\alpha!} z^\alpha \int_{\mathbb{S}_n} \xi^\alpha \bar{\xi}^\alpha d\sigma(\xi)$$
$$= \frac{d!}{\alpha!}\frac{\alpha!(n-1)!}{(d+n-1)!} z^\alpha$$
$$= \frac{d!(n-1)!}{(d+n-1)!} z^\alpha,$$

for $z \in \mathbb{B}_n$. Therefore, for $\alpha \in \mathbb{N}^n, |\alpha| = d$ we have

$$\int_{\mathbb{B}_n} w^\alpha \langle z,w\rangle^d \rho(w) dv(w)$$
$$= 2n \int_0^1 t^{2n-1+2d}\rho(t)dt \int_{\mathbb{S}_n} \xi^\alpha \langle z,\xi\rangle^d d\sigma(\xi)$$
$$= \frac{2d!n!\rho_{2n-1+2d}}{(d+n-1)!} z^\alpha, \qquad z \in \mathbb{B}_n.$$

It follows that

$$z^\alpha = \frac{(d+n-1)!}{2d!n!\rho_{2n-1+2d}} \int_{\mathbb{B}_n} w^\alpha \langle z,w\rangle^d \rho(w)dv(w), \tag{1}$$

for any $z \in \mathbb{B}_n$.

Since $\rho(t) > 0, 0 < t < 1$, for every $\varepsilon > 0$ there exists $C_\varepsilon > 0$ such that $\rho_s \geq C_\varepsilon(1-\varepsilon)^s$. Given $z \in \mathbb{B}_n$, we have

$$\int_{\mathbb{B}_n} \Big|\frac{1}{2}\sum_{d=0}^{\infty} \frac{(d+n-1)!}{d!n!\rho_{2n-1+2d}} \langle z,w\rangle^d\Big|^2 \rho(w)dv(w)$$
$$= \frac{1}{4}\sum_{d_1,d_2\geq 0} \frac{(d_1+n-1)!(d_2+n-1)!}{d_1!d_2!(n!)^2\rho_{2n-1+2d_1}\rho_{2n-1+2d_2}} \times$$
$$\times \int_{\mathbb{B}_n} \langle z,w\rangle^{d_1}\langle w,z\rangle^{d_2}\rho(w)dv(w)$$
$$= \frac{1}{4}\sum_{d_1,d_2\geq 0} \frac{(d_1+n-1)!(d_2+n-1)!}{d_1!d_2!(n!)^2\rho_{2n-1+2d_1}\rho_{2n-1+2d_2}} \times$$
$$\times \int_{\mathbb{B}_n} \sum_{|\beta|=d_2} w^\beta \bar{z}^\beta \frac{d_2!}{\beta!} \langle z,w\rangle^{d_1}\rho(w)dv(w)$$
$$= \frac{1}{2}\sum_{d\geq 0} \left(\frac{(d+n-1)!}{d!n!}\right) \frac{1}{\rho^2_{2n-1+2d}} \times$$
$$\times \sum_{|\beta|=d} \frac{(d!)^2}{\beta!}\frac{n!\rho_{2n-1+2d}}{(d+n-1)!} z^\beta \bar{z}^\beta$$
$$= \frac{1}{2}\sum_{d\geq 0} \frac{(d+n-1)!}{n!\rho_{2n-1+2d}} \sum_{|\beta|=d} \frac{z^\beta\bar{z}^\beta}{\beta!}$$
$$= \frac{1}{2}\sum_{d\geq 0} \frac{(d+n-1)!}{d!n!\rho_{2n-1+2d}} |z|^{2d} < \infty.$$

Thus, the function

$$w \mapsto \frac{1}{2}\sum_{d=0}^{\infty} \frac{(d+n-1)!}{d!n!\rho_{2n-1+2d}} \langle w,z\rangle^d$$

belongs to A^2_ρ.

By (1) and by continuity, for every $f \in A^2_\rho(\mathbb{B}_n)$, we have

$$f(z) = \int_{\mathbb{B}_n} f(w) \times$$
$$\times \left(\frac{1}{2}\sum_{d=0}^{\infty} \frac{(d+n-1)!}{d!n!\rho_{2n-1+2d}} \langle z,w\rangle^d\right) \rho(w)dv(w),$$

for $z \in \mathbb{B}_n$.

Therefore,

$$K_\rho(z,w) = \frac{1}{2}\sum_{d=0}^{\infty} \frac{(d+n-1)!}{d!n!\rho_{2n-1+2d}} \langle z,w\rangle^d.$$

□

3. PROOF OF MAIN RESULT

It suffices to consider only the case $n > 1$.

Proposition 3.1. *If $\rho \in \widehat{\mathcal{D}}$, then the projection $P_\rho : L^\infty \to \mathcal{B}$ is bounded, where P_ρ is defined by*

$$P_\rho\varphi(z) = \int_{\mathbb{B}_n} K_\rho(z,w)\varphi(w)\rho(w)dv(w),$$

for $\varphi \in L^\infty, z \in \mathbb{B}_n$.

https://doi.org/10.52111/qnjs.2022.16110

Proof. We have

$$K_\rho(z,w)=\frac{1}{2}\sum_{d=0}^{\infty}\frac{(d+n-1)!}{d!n!\rho_{2n-1+2d}}\langle z,w\rangle^d.$$

Hence, for a fixed $w\in\mathbb{B}_n$,

$$\begin{aligned}
&RK_\rho(z,w)\\
&=\sum_{j=1}^{n}z_j\frac{\partial K_\rho(z,w)}{\partial z_j}\\
&=\sum_{j=1}^{n}z_j\frac{\partial}{\partial z_j}\left(\frac{1}{2}\sum_{d=0}^{\infty}\frac{(d+n-1)!}{d!n!\rho_{2n-1+2d}}\langle z,w\rangle^d\right)\\
&=\frac{1}{2}\sum_{j=1}^{n}z_j\sum_{d=0}^{\infty}\frac{(d+n-1)!}{d!n!\rho_{2n-1+2d}}d\bar{w}_j\langle z,w\rangle^{d-1}\\
&=\frac{1}{2}\sum_{d=1}^{\infty}\frac{(d+n-1)!}{(d-1)!n!\rho_{2n-1+2d}}\langle z,w\rangle^d\\
&=\frac{1}{2}\sum_{d=1}^{\infty}\frac{\Gamma(d+n)}{\Gamma(d)\Gamma(n+1)\rho_{2n-1+2d}}\langle z,w\rangle^d.
\end{aligned}$$

Now, given $\varphi\in L^\infty$, let

$$\begin{aligned}
f(z)&:=P_\rho\varphi(z)\\
&=\int_{\mathbb{B}_n}K_\rho(z,w)\varphi(w)\rho(w)dv(w),
\end{aligned}$$

where $z\in\mathbb{B}_n$. For all $z\in\mathbb{B}_n$ we have

$$\begin{aligned}
\big|Rf(z)\big|&=\Big|\int_{\mathbb{B}_n}RK_\rho(z,w)\varphi(w)\rho(w)dv(w)\Big|\\
&\le\int_{\mathbb{B}_n}\big|RK_\rho(z,w)\big|\big|\varphi(w)\big|\,\rho(w)dv(w)\\
&\le\|\varphi\|_\infty\int_{\mathbb{B}_n}\big|RK_\rho(z,w)\big|\,\rho(w)dv(w).
\end{aligned}\tag{2}$$

Set

$$g(\lambda)=\sum_{d=1}^{\infty}\frac{\Gamma(d+n)}{\Gamma(d)}\frac{\lambda^{d-1}}{\rho_{2n-1+2d}},\qquad\lambda\in\mathbb{D}.$$

Since $\rho(t)>0, 0<t<1$, g is analytic on the unit disk. Then

$$RK_\rho(z,w)=\frac{\langle z,w\rangle}{2\Gamma(n+1)}g(\langle z,w\rangle).\tag{3}$$

Next we consider the reproducing kernel $K^1_\rho(z,w)$ of the Bergman space in the unit disk with the weight ρ. We have

$$K^1_\rho(z,w)=\frac{1}{2}\sum_{d=0}^{\infty}\frac{(z\overline{w})^d}{\rho_{2d+1}}.$$

Furthermore,

$$\begin{aligned}
\frac{\partial^n}{\partial z^n}K^1_\rho(z,w)&=\frac{1}{2}\sum_{d=n}^{\infty}\frac{\Gamma(d+1)(z\overline{w})^{d-n}\overline{w}^n}{\Gamma(d-n+1)\rho_{2d+1}}\\
&=\frac{1}{2}\sum_{s=1}^{\infty}\frac{\Gamma(s+1)}{\Gamma(s)}\frac{(z\overline{w})^{s-1}\overline{w}^n}{\rho_{2s+2n-1}}\\
&=\frac{1}{2}g(z\overline{w})\overline{w}^n.
\end{aligned}$$

By a result of Peláez and Rättyä ([7] Theorem 1 (ii)), we have

$$\begin{aligned}
&\int_{\mathbb{D}}\Big|\frac{\partial^n}{\partial z^n}K^1_\rho(z,w)\Big|(1-|z|^2)^{n-2}dA(z)\\
&\asymp\int_0^{|w|}\frac{dt}{\widehat{\rho}(t)(1-t)^2},\qquad\frac{1}{2}\le|w|<1,
\end{aligned}$$

where $\widehat{\rho}(t)=\int_t^1\rho(s)ds$.

Thus,

$$\begin{aligned}
&\int_{\mathbb{D}}\big|g(z\overline{w})\big|\,(1-|z|^2)^{n-2}dA(z)\\
&\asymp\int_0^{|w|}\frac{dt}{\widehat{\rho}(t)(1-t)^2},\qquad\frac{1}{2}\le|w|<1.
\end{aligned}$$

Since g is analytic on the unit disk, we have

$$\begin{aligned}
&\int_{\mathbb{D}}\big|g(z\overline{w})\big|\,(1-|z|^2)^{n-2}dA(z)\\
&\lesssim 1+\int_0^{|w|}\frac{dt}{\widehat{\rho}(t)(1-t)^2},\qquad w\in\mathbb{D}.
\end{aligned}\tag{4}$$

Now, by (3), we have

$$\int_{\mathbb{B}_n}\big|RK_\rho(z,w)\big|\,\rho(w)dv(w)$$

$$\lesssim \int_{\mathbb{B}_n} \big|g(\langle z,w\rangle)\big|\,\rho(w)dv(w)$$
$$\asymp \int_0^1 r^{2n-1}\rho(r)\left(\int_{\mathbb{S}_n}\big|g(\langle rz,\xi\rangle)\big|\,d\sigma(\xi)\right)dr.$$

By[9] Lemma 1.9 and the unitary invariance of $d\sigma$, we have

$$\int_{\mathbb{S}_n}\big|g(\langle rz,\xi\rangle)\big|\,d\sigma(\xi) \asymp \int_{\mathbb{D}}\big|g(r|z|\,\lambda)\big|\,(1-|\lambda|^2)^{n-2}dA(\lambda).$$

Thus, by (4) we obtain

$$\int_{\mathbb{B}_n}\big|RK_\rho(z,w)\big|\,\rho(w)dv(w)$$
$$\lesssim \int_0^1 r^{2n-1}\rho(r)\left(1+\int_0^{r|z|}\frac{dt}{\widehat{\rho}(t)(1-t)^2}\right)dr$$
$$\lesssim 1+\int_0^{|z|}\frac{1}{\widehat{\rho}(t)(1-t)^2}\left(\int_{t/|z|}^1 r^{2n-1}\rho(r)dr\right)dt$$
$$\lesssim 1+\int_0^{|z|}\frac{\widehat{\rho}(t/|z|)}{\widehat{\rho}(t)}\frac{dt}{(1-t)^2}$$
$$\lesssim \frac{1}{1-|z|},\qquad z\in\mathbb{B}_n.$$

By (2) we obtain now that

$$\big|Rf(z)\big|\lesssim\|\varphi\|_\infty\frac{1}{1-|z|^2},\quad z\in\mathbb{B}_n.$$

Hence,

$$\sup_{z\in\mathbb{B}_n}(1-|z|^2)\big|Rf(z)\big|\lesssim\|\varphi\|_\infty.$$

It is easy to see that

$$\big|f(0)\big|\lesssim\|\varphi\|_\infty.$$

Therefore, P_ρ is bounded. The Proposition 3.1 is proved. □

Proposition 3.2. *Suppose that the projection $P_\rho: L^\infty\to\mathcal{B}$ is bounded. Then $\rho\in\widehat{\mathcal{D}}$.*

Proof. Given $\xi\in\mathbb{S}_n$ and $w\in\mathbb{B}_n$, let us consider a function g given by

$$g(\lambda)=RK_\rho(\lambda\xi,w),\qquad \lambda\in\mathbb{D}.$$

Then

$$g(\lambda)=\sum_{d=1}^\infty c_d\langle\xi,w\rangle^d\lambda^d,$$

where $c_d=\dfrac{1}{2n}\dfrac{\Gamma(d+n)}{\Gamma(d)\Gamma(n)\rho_{2n-1+2d}}$.

By the Hardy–Littlewood inequality (see Lemma 2.2) we have

$$\sum_{d=1}^\infty\frac{c_d\big|\langle\xi,w\rangle\big|^d}{d+1}\lesssim\int_0^{2\pi}\Big|g(e^{i\theta})\Big|\,\frac{d\theta}{2\pi}$$
$$=\int_0^{2\pi}\Big|RK_\rho(e^{i\theta}\xi,w)\Big|\,\frac{d\theta}{2\pi}.$$

Integrating both sides of the above inequality over $\xi\in\mathbb{S}_n$ we obtain

$$\sum_{d=1}^\infty\frac{c_d}{d+1}\int_{\mathbb{S}_n}\big|\langle\xi,w\rangle\big|^d\,d\sigma(\xi)$$
$$\lesssim\int_{\mathbb{S}_n}\int_0^{2\pi}\Big|RK_\rho(e^{i\theta}\xi,w)\Big|\,\frac{d\theta}{2\pi}d\sigma(\xi)$$
$$=\int_{\mathbb{S}_n}\big|RK_\rho(\xi,w)\big|\,d\sigma(\xi).$$

By the unitary invariance of $d\sigma$ and[9] Lemma 1.9, we have

$$\int_{\mathbb{S}_n}\big|\langle\xi,w\rangle\big|^d\,d\sigma(\xi)$$
$$=|w|^d\int_{\mathbb{S}_n}|\xi_1|^d\,d\sigma(\xi)$$
$$=(n-1)|w|^d\int_{\mathbb{D}}(1-|z|^2)^{n-2}|z|^d\,dA(z)$$
$$=(n-1)\pi|w|^d\int_0^1(1-t)^{n-2}t^{d/2}dt$$
$$\asymp\frac{\Gamma(\frac{d}{2}+1)\Gamma(n)}{\Gamma(\frac{d}{2}+n)}|w|^d.$$

Hence,

$$\int_{\mathbb{S}_n}\big|RK_\rho(\xi,w)\big|\,d\sigma(\xi)$$
$$\gtrsim\sum_{d=1}^\infty\frac{c_d}{d+1}\frac{\Gamma(\frac{d}{2}+1)\Gamma(n)}{\Gamma(\frac{d}{2}+n)}|w|^d$$

https://doi.org/10.52111/qnjs.2022.16110

$$= \frac{1}{2n}\sum_{d=1}^{\infty}\frac{\Gamma(d+n)\Gamma(\frac{d}{2}+1)}{(d+1)\Gamma(d)\Gamma(\frac{d}{2}+n)\rho_{2n-1+2d}}|w|^d.$$

Since

$$\frac{\Gamma(d+n)\Gamma(\frac{d}{2}+1)}{(d+1)\Gamma(d)\Gamma(\frac{d}{2}+n)} \asymp 1,$$

we get

$$\int_{\mathbb{S}_n}\left|RK_\rho(\xi,w)\right|\,d\sigma(\xi) \gtrsim \frac{1}{2n}\sum_{d=1}^{\infty}\frac{|w|^d}{\rho_{2n-1+2d}}, \qquad w\in\mathbb{B}_n.$$

Therefore, for $z\in\mathbb{B}_n$, we have

$$\begin{aligned}
&\int_{\mathbb{B}_n}\left|RK_\rho(z,w)\right|\rho(w)dv(w)\\
&= 2n\int_0^1 r^{2n-1}\rho(r)\int_{\mathbb{S}_n}\left|RK_\rho(z,r\xi)\right|\,d\sigma(\xi)\,dr\\
&= 2n\int_0^1 r^{2n-1}\rho(r)\int_{\mathbb{S}_n}\left|RK_\rho(\xi,rz)\right|\,d\sigma(\xi)\,dr\\
&\gtrsim \sum_{d=1}^{\infty}\frac{|z|^d}{\rho_{2n-1+2d}}\int_0^1 r^{2n-1+d}\rho(r)dr\\
&= \sum_{d=1}^{\infty}\frac{\rho_{2n-1+d}}{\rho_{2n-1+2d}}|z|^d.
\end{aligned}$$

Thus,

$$\begin{aligned}
&\sup_{z\in\mathbb{B}_n}(1-|z|^2)\int_{\mathbb{B}_n}\left|RK_\rho(z,w)\right|\rho(w)dv(w)\\
&\gtrsim \sup_{z\in\mathbb{B}_n}(1-|z|)\sum_{d=1}^{\infty}\frac{\rho_{d+2n-1}}{\rho_{2d+2n-1}}|z|^d\\
&\geq \sup_{N\in\mathbb{N}}\frac{1}{N}\sum_{d=1}^{N}\frac{\rho_{d+2n-1}}{\rho_{2d+2n-1}}\left(1-\frac{1}{N}\right)^d\\
&\gtrsim \sup_{N\in\mathbb{N}}\frac{1}{N}\sum_{d=1}^{N}\frac{\rho_{d+2n-1}}{\rho_{2d+2n-1}}.
\end{aligned}$$

Since P_ρ is bounded,

$$\sup_{z\in\mathbb{B}_n}(1-|z|^2)\int_{\mathbb{B}_n}\left|RK_\rho(z,w)\right|\rho(w)dv(w)<\infty.$$

Given $N\geq 2n$, we obtain that

$$\begin{aligned}
1 &\gtrsim \frac{1}{4N-2n}\sum_{d=3N-n+1}^{4N-2n}\frac{\rho_{d+2n-1}}{\rho_{2d+2n-1}}\\
&\geq \frac{1}{4N}(N-n)\frac{\rho_{4N}}{\rho_{6N}}.
\end{aligned}$$

Hence,

$$\rho_{6N}\gtrsim\rho_{4N}.$$

If $8N\leq k<8N+8, N\geq 2n+8$, then

$$\rho_k\leq\rho_{8N}\lesssim\rho_{12N}\lesssim\rho_{18N}\leq\rho_{2k}.$$

On the other hand, since ρ is positive and integrable on $[0,1)$, it is easy to see that

$$\widehat{\rho}(0)\leq C_0\widehat{\rho}(\frac{1}{2})$$

for some $C_0>0$.

Hence, by Lemma 2.1 we conclude that $\rho\in\widehat{\mathcal{D}}$. □

From Proposition 3.1 and Proposition 3.2, we obtain the conclusion of Theorem 1.1.

Remark 3.3. The method given herein combined with our results in[5] can be used to generalize to the unit ball case the L^p estimates proved in[7] in the unit disk case. This will be the object of a forthcoming paper.

Acknowledgement

This study is conducted within the framework of science and technology projects at institutional level of Quy Nhon University under the project code T2021.700.03.

I am grateful to Alexander Borichev and El Hassan Youssfi for helpful remarks.

REFERENCES

1. O. Constantin, J. A. Peláez. Boundedness of the Bergman projection on L^p spaces with exponential weights, *Bulletin des Sciences Mathematiques*, **2015**, *139*, 245–268.

2. M. Dostanić. Unboundedness of the Bergman projections on L^p spaces with exponential weights, *Proceedings of the Edinburgh Mathematical Society*, **2004**, *47*(1), 111–117.

3. M. Dostanić. Boundedness of the Bergman projections on L^p spaces with radial weights, *Publications de l'Institut Mathematique*, **2009**, *86*, 5–20.

4. P. L. Duren. *Theory of H^p Spaces*, Academic Press, 1970.

5. V. A. Le. Carleson measures and Toeplitz operators on small Bergman spaces on the ball, *Czechoslovak Mathematical Journal*, **2021**, *71*(1), 211–229.

6. J. A. Peláez. Small weighted Bergman spaces, *Proceedings of the summer school in complex and harmonic analysis, and related topics*, Publications of the University of Eastern Finland - Reports and Studies in Forestry and Natural Sciences, Joensuu **2016**, 29–98.

7. J. A. Peláez, J. Rättyä. Two weight inequality for Bergman projection, *Journal de Mathématiques Pures et Appliquées*, **2016**, *105*(1), 102–130.

8. J. A. Peláez, J. Rättyä. Bergman projection induced by radial weight, *Advances in Mathematics*, **2021**, *391*, 107950.

9. K. Zhu. *Spaces of Holomorphic Functions in the Unit Ball*, Springer-Verlag, New York, 2005.

10. K. Zhu, *Operator Theory in Function Spaces*, 2nd edition, American Mathematical Society, Providence, Rhode Island, 2007.

https://doi.org/10.52111/qnjs.2022.16110

JOURNAL OF SCIENCE
QUY NHON UNIVERSITY
http://js.qnu.edu.vn
Vol. 16, N° 1, 2022
ISSN : 1859-0357

CONTENTS